Supporting Information

Berna et al. 10.1073/pnas.1117620109

SI Text

Archeological Stratigraphic Sequence in Excavation 1. A plan of excavation 1 is given in Fig. S1. Archaeological strata were defined by Beaumont during excavation (1). In publications, Beaumont presents subdivisions of Strata (St.)—St.12 a-c; 10a-b; 9a-f; 8a-e;7a-b; 5a-b—but the basis for these subdivisions has not been described by him, nor is it possible to pinpoint the transitions between subdivisions in the stratigraphic profiles. As a consequence, we have grouped artifacts by strata. It is however possible to track depth within the stratum for each artifact.

Presentations of Wonderwerk Cave by Beaumont (i.e., refs. 1, 2) also use site-wide Major Units, which are based on strata-specific correlations between excavation areas. The correlations, however, are not based on detailed lithic, faunal, or botanical analyses, continuous stratigraphic profiles, or rigorous absolute dates, so we have chosen not to adopt the Major Units described by Beaumont, and we treat each excavation area separately based on its excavation-specific strata.

The lithic assemblage from Beaumont's excavation is curated in the McGregor Museum, Kimberley (South Africa). This sample includes all lithic material recovered during excavation and is dominated by fragments of dolostone from roof collapse in addition to artifacts and manuports. Throughout the sequence of excavation 1, the lithic assemblage size is small and the number of flakes is very limited. All flaked material and pieces with pot-lid fracture were cataloged for documentation and analysis.

Stratum 12. The lithic assemblage of stratum 12 is characterized by small flakes and small cores (3). This assemblage is assigned to the Oldowan and appears comparable to the assemblage from Sterkfontein, although there is a significant difference in raw material between Sterkfontein where the dominant material is quartzite and Wonderwerk stratum 12, where the dominant raw material is chert.

Stratum 11. Stratum 11 has yielded a very small assemblage of only two bifaces and 19 tools in total (3). One biface (SPL 37) that was found near the base of stratum 11 is very crudely worked and is best classified as a protobiface (Fig. S2*A*). The definition of a protobiface, following Leakey (4), includes bifacial flaking along both edges and at the tip. On SPL 37, bifacial flaking is limited to one edge and the tip; however, the nature of the fine removals on the tip fits better with the classification of a protobiface than with classification as a chopper. The second biface (SPL 36) was recovered near the top of the stratum and is characterized by a series of short removals around the circumference. The tip is broken and the piece is damaged by conchoidal fractures associated with the development of calcium carbonate crusts.

Stratum 10. Seven bifaces were recovered from stratum 10 (Fig. 1 *B* and *C* and Fig. S3 *A*–*D*). With one exception, none of the bifaces show invasive flake scars. Biface tips tend to be cleaver-like, as they form a working edge rather than a pointed tip, although the overall dimensions of the bifaces do not fit with the definition for cleavers. All are on slabs of ironstone, with the exception of two bifaces (SPL 39 and 702), which are on large cortical flakes (Fig. S3 *B* and *D*). One piece (SPL 45) included as a biface could be classified as a chopper, as it consists of three large removals with deep bulbs of percussion on an ironstone cobble (Fig. S3*C*). Several of the bifaces have more than one working edge. The most striking of these is SPL 702 (Fig. S3*D*), which is on a large semicortical flake of homogenous gray ironstone. This biface is trapezoidal in section, with one edge formed by a preexisting dorsal flake scar and the other by abrupt removals off the opposing edge. There are just a few invasive flake scars, all with prominent bulbs. The tip is offset from the main axis and has been formed with a series of flat removals off one face. There is also limited working on the base which has a cleaver-like edge that is quite sharp. From a functional perspective, this can be seen as a double cleaver/handaxe tool. There are a total of 36 flakes and 15 cores from stratum 10; however, none of these can be considered diagnostic of a specific production method. As shown in Fig. S1, the bifaces are mostly found in the central and southern part of the excavated area in excavation 1, whereas flakes are more widely distributed.

Strata 9 and 8. Beginning with stratum 9, there is decrease in biface thickness and increase in length-to-thickness ratio (i.e., refinement) associated with the development of invasive flat removals for thinning bifaces which first appears in stratum 9 and then becomes a regular aspect of the assemblage in stratum 8. In the upper part of stratum 9 and in stratum 8, there are several cleavers that appear consistent with the Victoria West technique, as they are made on large flakes struck from apparently prepared cores (5). One of these cleavers is made on igneous rock (Fig. S2*B*). One handaxe from stratum 8 is made on chert, the first large tool on this raw material in the sequence (Fig. S2*C*). Throughout the sequence assemblage size is small and the number of flakes is very limited. There is no evidence of either reduction in biface size in the excavation 1 sequence or systematic blade production that would support the attribution of stratum 8 to stratum 5 to the Fauresmith (1).

Chronostratigraphic Sequence in Excavation 1. Paleomagnetic orientation and cosmogenic $^{26}Al/^{10}Be$ ratio were analyzed along the excavation 1 sequence in the main north and main east profiles (Fig. S1). An integrated overview of the paleomagnetic data and the cosmogenic dates from the stratigraphic sequence is given in Fig. S4. The burial ages calculated from the measured $^{26}Al/^{10}Be$ ratio are given in Table S1. These ages are calculated using $^{26}Al/^{10}Be$ ratios of 3.98 ± 0.24 and 4.08 ± 0.22 of samples collected from the surface outside the cave, which imply an initial burial signal corresponding to 0.78 ± 0.15 Ma (see ref. 6).

SI Materials and Methods

Faunal Sample. A sample of mammalian bones and teeth, representing just more than one quarter of the total stratum 10 faunal assemblage, has been studied to date. For each item, surface color was scored by using five categories that have been shown to follow a progression during burning (7, 8) (Table S2): brown-red, black, gray-white, and white (i.e., calcined).

Heat Experiment with Lithic Raw Material. Four slabs of local ironstone were collected from outside Wonderwerk Cave and cut with a petrographic saw into four subsamples, each approximately 2 × 2 × 1 cm in size. Subsamples from each slab were heated in a programmable laboratory kiln to temperatures of 250 °C, 500 °C, 750 °C, and 1,000 °C, respectively, for a duration of 1 hour. The samples were then examined for changes to color and texture as well as the presence and characteristics of pot-lid fractures (Fig. S7).

Botany. Three samples of macrobotanical remains were analyzed from stratum 10. Two derive from square R25 and one is from square T33 (Fig. S9).

Grass culm. The epidermis has been partially removed from the culm, revealing several longitudinal peripheral vascular bundles. This fragment is 3 mm long and just less than 1 mm in diameter. Another fragment is 0.5 mm in diameter and has a solid outer

cortex with large cells toward the center that form a central canal or more likely a central hollow because the cells have broken down.

Sedge culm. Another two examples with a diameter of 0.7 mm have a very thin epidermis and aerenchymatous cells in the center (like a sponge). The vascular bundles are not visible. The sedge *Eleocharis* spp. has this type of culm.

Dicot stem or root. These are also 0.5 and 0.7 mm in diameter, but have a different type of tissues. They typically crack radially (i.e., like slices of a pie) and comprise fibers and parenchyma as the ground tissue (i.e., smallest cells), with solitary vessels (i.e., larger empty cells). It is not possible to identify such small-diameter stems or roots.

1. Beaumont PB, Vogel JC (2006) On a timescale for the past million years of human history in central South Africa. *S Afr J Sci* 102:217–228.
2. Beaumont PB (2011) The edge: more on fire-making by about 1.7 million years ago at Wonderwerk Cave in South Africa. *Curr. Ant.* 52:585–595.
3. Chazan M, et al. (2008) Radiometric dating of the Earlier Stone Age sequence in excavation I at Wonderwerk Cave, South Africa: preliminary results. *J Hum Evol* 55: 1–11.
4. Leakey M (1971) *Olduvai Gorge: Excavations in Beds I and II, 1960-1963* (Cambridge Univ Press, Cambridge).
5. Lycett SJ, von Cramon-Taubadel N, Gowlett JAJ (2010) A comparative 3D geometric morphometric analysis of Victoria West cores: Implications for the origins of Levallois technology. *J. Arch. Sci.* 37:1110–1117.
6. Matmon A, et al. (2012) Reconstructing the history of sediment deposition in caves: A case study from Wonderwerk Cave, South Africa. *Geol Soc Am Bull* 124:611–625.
7. Stiner MC (1991) The faunal remains from Grotta Guattari: A taphonomic perspective. *Curr. Anth.* 32:103–117.
8. Stiner MC, Weiner S, Bar-Yosef O, Kuhn S (1995) Differential burning, fragmentation, and preservation of archaeological bone. *J. Arch. Sci* 22:223–237.

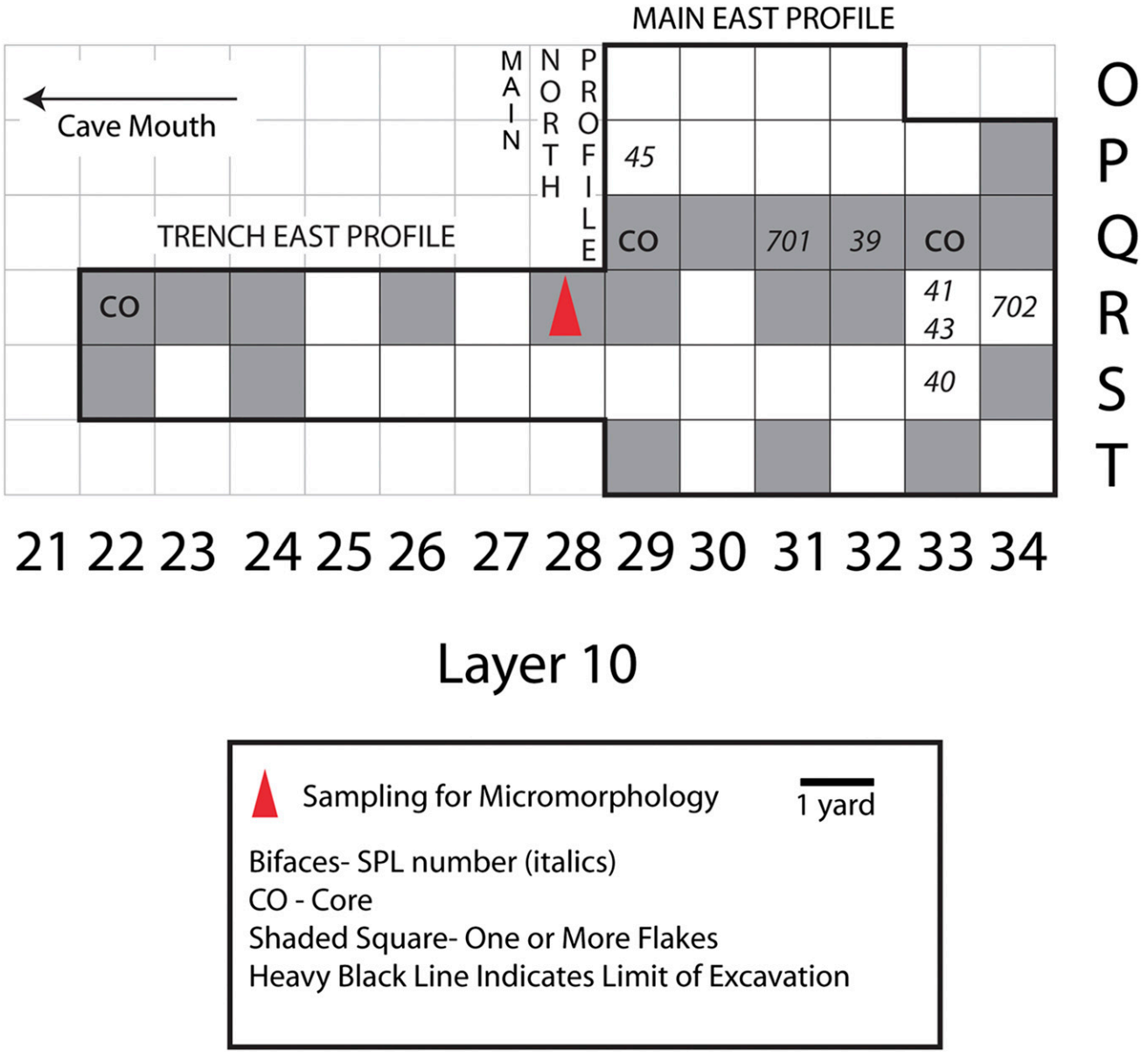

Fig. S1. Distribution of artifacts in stratum 10, excavation 1, in Wonderwerk Cave, relative to the location where micromorphology revealed the presence of ashed plant material (red arrow).

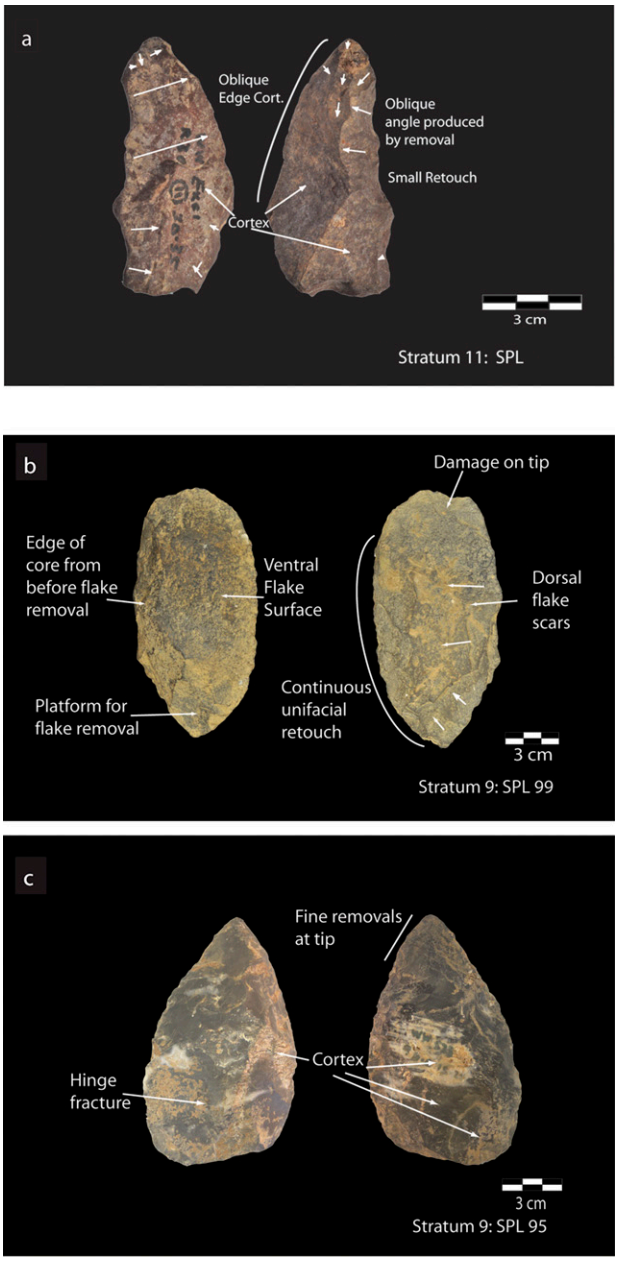

Fig. S2. Bifaces from excavation 1, Wonderwerk Cave: (*A*) stratum 11 and (*B* and *C*) stratum 9.

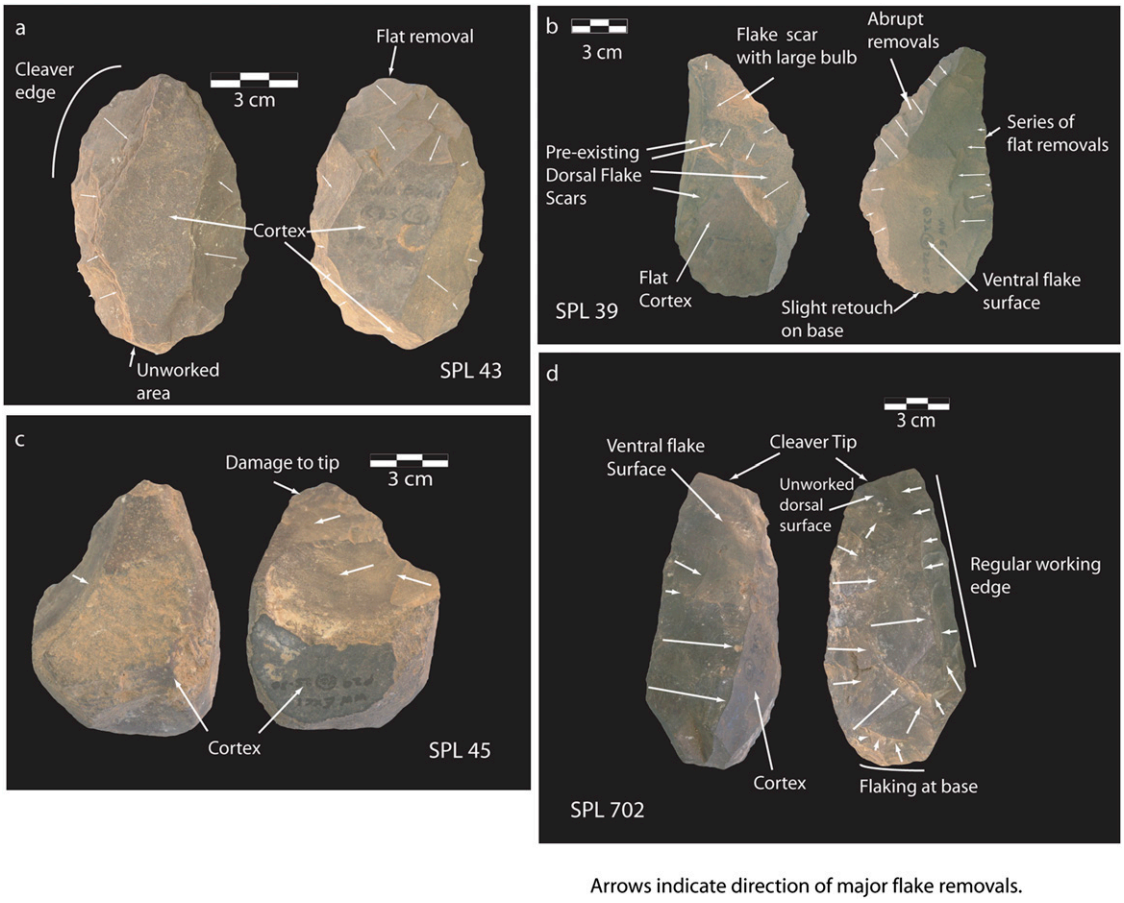

Fig. S3. Bifaces from stratum 10, excavation 1, Wonderwerk Cave. (*A*) SPL 43 on slab of ironstone. (*B*) SPL 39 on a large semicortical flake of homogenous gray ironstone. (*C*) SPL 45 on ironstone cobble. (*D*) SPL 702 on large ironstone cortical flake.

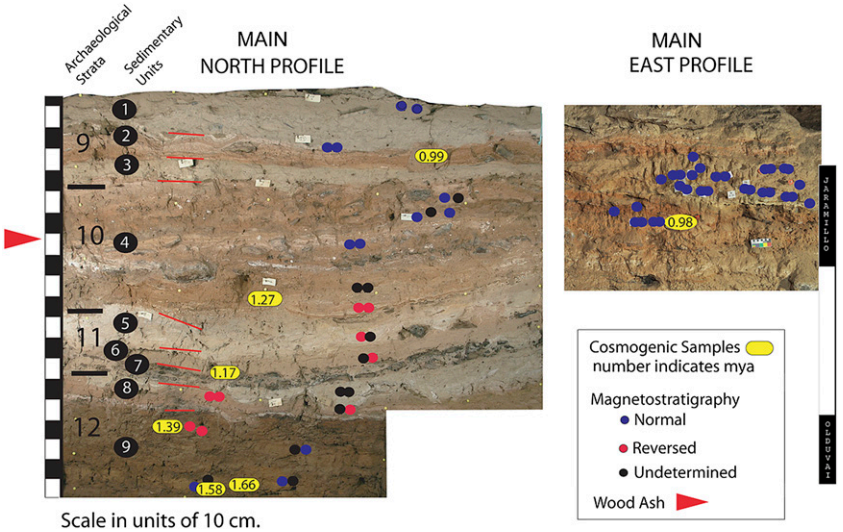

Fig. S4. Photograph of main north and main east profiles of excavation 1 show subdivision of archaeological strata 12 to 9, the corresponding sedimentary units (i.e., numbers 1–9), and the locations of cosmogenic dates (in yellow boxes) and paleomagnetic normal and reverse data (black circle, undetermined; red circle, reverse; blue circle, normal). Further details can be found in refs. 3, 6.

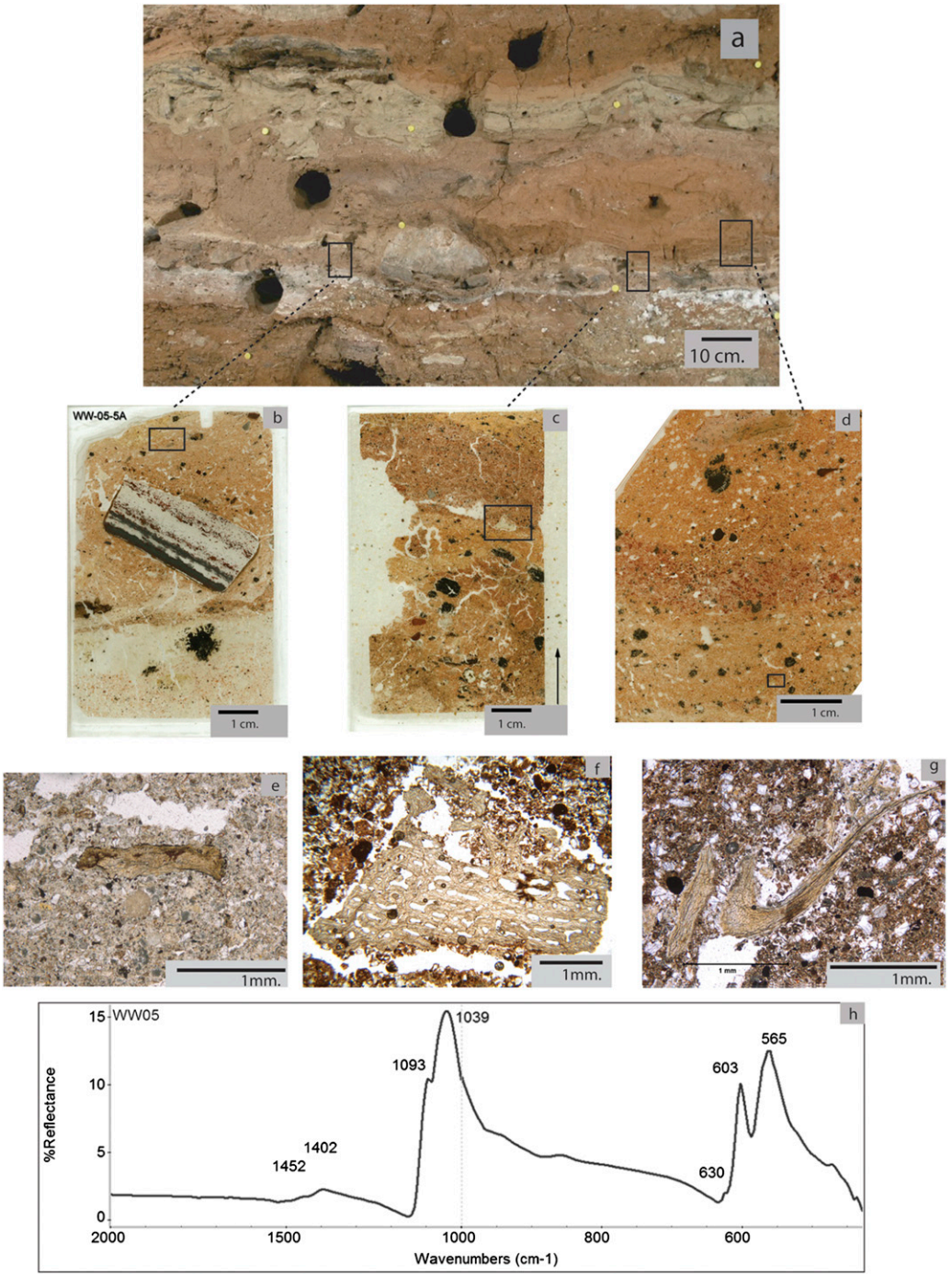

Fig. S5. (*A*) Photograph of stratum 10 in the trench east profile of excavation 1. Boxes mark approximate locations of thin sections shown in images *B*–*D*. (*B*) Scan of 5 × 7.5 cm petrographic thin section showing two major microstratigraphic units. (*i*) At bottom, there is white phosphatized flowstone or degraded dolomite with iron manganese dendritic nodules. (*ii*) At top, separated by sharp boundary, is orange-red sand with few partially disaggregated rounded silt aggregates and millimeter-sized bone fragments and opaque millimeter-size oxide nodules. Note a large angular fragment of ironstone. Small dashed box indicates location of bone fragments shown in micrograph [*E*; plane-polarized (PPL)] (Scale bar: 1 cm). (*C*) Scan of 5 × 7.5 cm petrographic thin section showing two major microstratigraphic units separated by a sharp contact onto which large (i.e., centimeter-size) fragments of bone were deposited. The unit at the bottom (*i*) is composed of a dusty silty clay groundmass, with quartz grains coated with clay and local impregnations of Fe-Mn. The top portion of the unit is locally bedded with some phytoliths. (In cross-polarized light; not shown here—the sand beneath the contact appears compressed, as if it were trampled.) In the top unit (*ii*), several bone fragments and phosphatized wood ash fragments are present. Small dashed box indicates location of bone fragments shown in micrograph. (*D*) Scan of petrographic thin section exhibiting three microstratigraphic units: (*i*) bottom sand silt and clay mixed with ashed plant material, dispersed wood ash, and bone fragments; (*ii*) reddish clay aggregates and fragments; and (*iii*) rounded aggregates of sandy silt. Small dashed box indicates location of bone fragments shown in micrograph (*G*). (*E*) Micrograph of charred bone (PPL). (Scale bar: 1 mm.) (*F*) Micrograph of white spongy bone fragment laying on the surface between two microstratigraphic units (PPL). (Scale bar: 1 mm.) (*G*) Angular fragments of partially charred bone (PPL). (Scale bar: 1 mm.) (*H*) Representative reflectance Fourier transform IR microspectroscopy spectra collected from bone fragments in micrographs *E*–*G* showing the presence of IR bands at 630 cm^{-1} and 1,090 cm^{-1} characteristic of bone mineral heated above 400 °C.

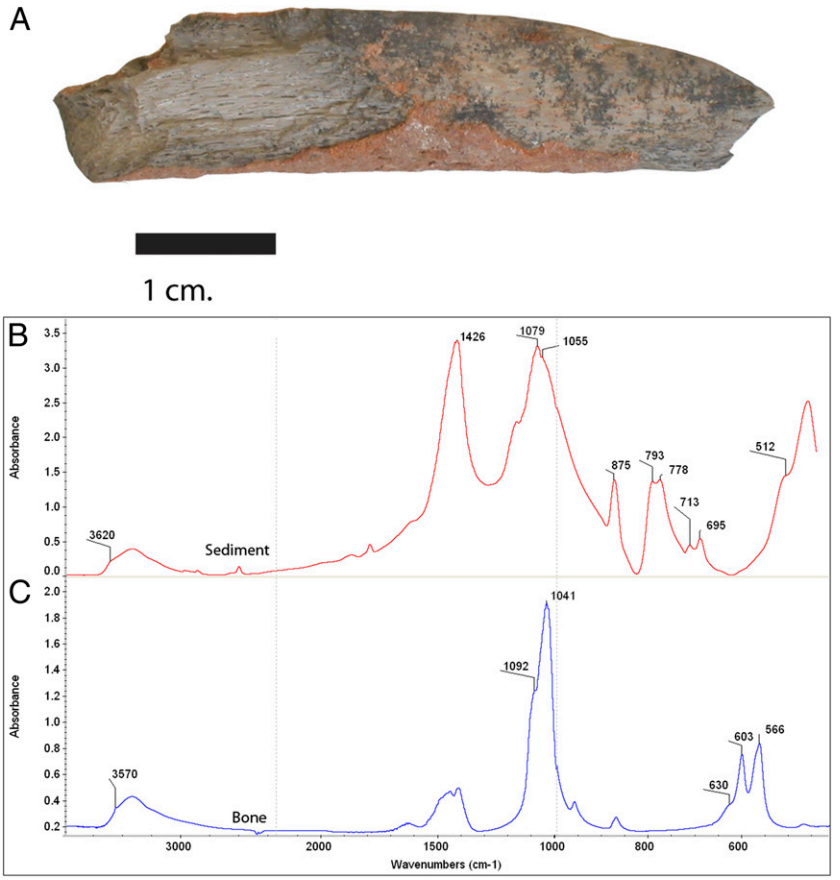

Fig. S6. (*A*) Fragment of discolored (gray) bone with adhering rubefied sediment from excavation 1, stratum 10, square Q31. (*B*) Representative Fourier transform IR spectrum of rubefied sediment showing IR pattern characteristic of quartz, calcite, and heat-altered clay as described previously (1). (*C*) Representative Fourier transform IR spectrum of the gray bone material showing presence of IR absorptions at 630, 1,090, and 3,570 cm^{-1} characteristic of bone mineral heated above 400 °C.

1. Berna F, et al. (2007) Sediments exposed to high temperatures: Reconstructing pyrotechnological practices in Late Bronze and Iron Age Strata at Tel Dor (Israel). *J. Arch. Sci.* 34:358–373.

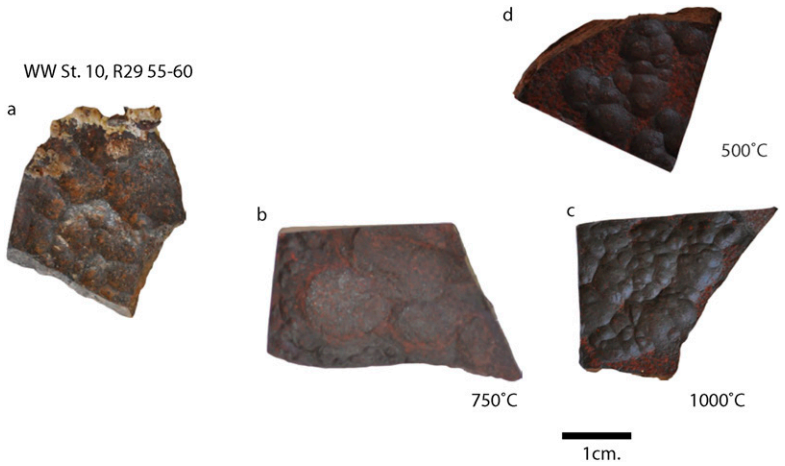

Fig. S7. (*A*) Photograph of banded ironstone fragment from location adjacent to wood ash (Square R28). Note characteristic pot-lid fracture. (*B–D*) Samples of banded ironstone slabs collected on the hillside outside Wonderwerk Cave and heated under experimental conditions at temperatures ranging from 500 °C to 1000 °C for one hour, showing the formation of pot-lid fractures comparable to the ones found in the archaeological assemblage.

Fig. S8. Ironstone slabs with refitted pot-lid flake from excavation 1, stratum 10, square Q33, spit 10 to 15 cm.

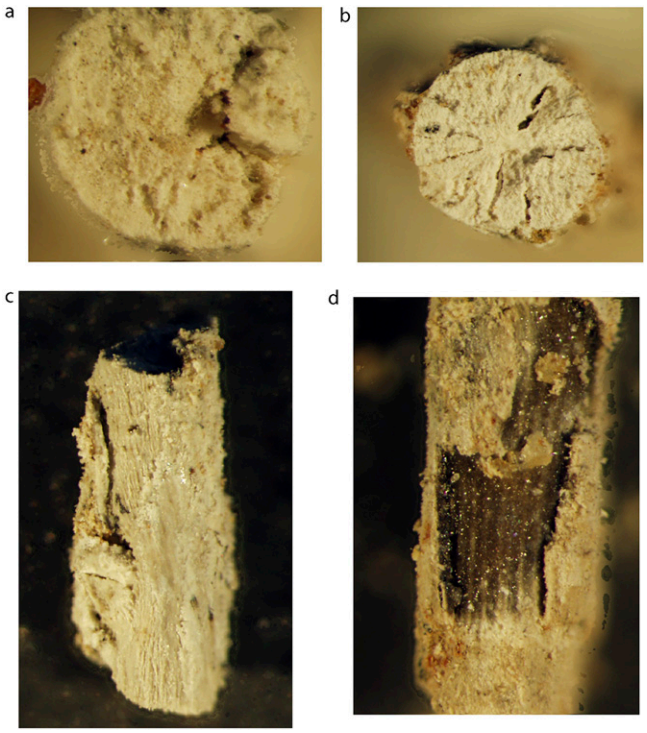

Fig. S9. Macrobotanical remains from stratum 10. (*A*) Culm with a diameter of 0.7 mm, very thin epidermis, and aerenchymatous cells in the center. The vascular bundles are not visible. The sedge *Eleocharis* spp. has this type of culm. (*B*) Dicot stem or root, 0.5 and 0.7 mm in diameter, with different type of tissues. Dicots typically crack radially and comprise fibers and parenchyma as the ground tissue (i.e., smallest cells), with solitary vessels (i.e., larger empty cells). It is not possible to identify such small-diameter stems or roots. (*C*) Dicot stem or root external view with a knot where a "branch" was attached. (*D*) Grass culm: the epidermis has been partially removed from the culm, revealing several longitudinal peripheral vascular bundles (light lines in a dark background). This fragment is 3 mm long and just less than 1 mm in diameter.

Table S1. Cosmogenic burial ages for excavation 1, based on $^{26}Al/^{10}Be$ ratio measured in sediment samples collected along the stratigraphic column

Sample	Archaeological stratum	Sedimentary unit	Age, Myr
COS 6	9	2	0.99 ± 0.19
COS 5	10	4 top	0.98 ± 0.19
COS 4	10	4	1.27 ± 0.19
COS 3	11	6	1.17 ± 0.19
COS 2	12	9 top	1.39 ± 0.19
COS 1	12	9 bottom	1.66 ± 0.20
WWD 1	12	9 bottom	1.58 ± 0.19

For complete discussion of these ages see Matmon et al (6).

Table S2. Burned and unburned bone and teeth from a sample of fauna recovered from stratum 10 in excavation 1 at Wonderwerk Cave and a breakdown of burned bone by color

	NISP bone	% bone	NISP teeth	% teeth	Teeth and bone NISP
Unburned	349	91.8	31	8.2	380
Burned	246	83.3	49	16.6	295
Total	595	88.1	80	11.8	675

Burning color	NISP bone	% of total bone	NISP teeth	% of total teeth	Teeth and bone NISP
Brown-red	6	1.0	2	2.5	8
Black	58	9.7	33	41.2	91
Grey	103	17.3	14	17.5	117
White	79	13.2	0	0	79

NISP, number of identified specimens.